

Acoustic impedance inversion of vintage seismic data over a proposed CO₂ sequestration site in the Lake Wabamun Area, Alberta

Abdullah Alshuhail, Don Lawton and Helen Isaac

ABSTRACT

Seismic inversion of the Nisku Formation in the Lake Wabamun area has revealed contrasts in acoustic impedance caused by lateral changes in lithology and/or porosity of the Nisku Formation. This interpretation is constrained by well control and supported by seismic modelling, which suggests that changes in Nisku thickness over the range encountered in the study area has only a small effect on acoustic impedance. Thus, acoustic impedance mapping may provide one approach in pursuing favourable sites for CO₂ injection in addition to the conventional time structure, amplitude maps and other seismic attributes. Our analysis revealed favourable low-impedance, high-porosity locations that could be potential injection sites.

INTRODUCTION

The province of Alberta contributes more than 30% to the total Canadian CO₂ emissions, according to recent statistics by Environment Canada (2007). In an effort to offset the carbon emissions and meet up with potential increase in energy demands, several CO₂ sequestration projects were recently launched in the province. These include the Alberta Saline Aquifer CO₂ Project (ASAP), the Heartland Area CO₂ Sequestration Project (HARP), and the Wabamun Area CO₂ Project (WASP).

In the Lake Wabamun Area, the Nisku Formation has been advocated as a sink for large-scale CO₂ sequestration project (Michael et al., 2008) with capacity in the order of a megaton per year. Therefore, seismic characterization is being undertaken as part of Phase I of WASP to: (1) generate detailed attribute maps of the Nisku Formation, (2) provide indications of variations in its porosity and lithology, and (3) delineate any potential geologic risks in the area that may compromise the integrity of the Nisku Formation as a CO₂ sink. This report outlines some of the results from the ongoing seismic characterization pertaining to the acoustic impedance inversion.

STUDY AREA

The study area is located approximately 50 km southwest of Edmonton in the vicinity of the Lake Wabamun Area in the central plains of Alberta, Canada (Figure 1). The injection target is the Devonian brine-bearing Nisku dolostone formation. The formation was deposited at the edge of carbonate shelf and its lithology becomes interbedded with limestone and shale as we move to the northwest direction (Watts, 1987). The Nisku Formation is confined between two aquitards (Figure 2) and its depth and thickness range from 1800 - 2200 m and 40 - 80 m, respectively. Furthermore, the overlying Calmar shale makes a good cap rock which prevents injected CO₂ from seeping into the surface or into shallow aquifers. In addition, the Nisku aquifer properties, such as temperature and salinity, make it a favourable candidate for CO₂ storage (Michael et al., 2008). The

seismic characterization is constrained to a high-grade focus area, where favourable conditions in terms of seismic coverage and other factors exist.

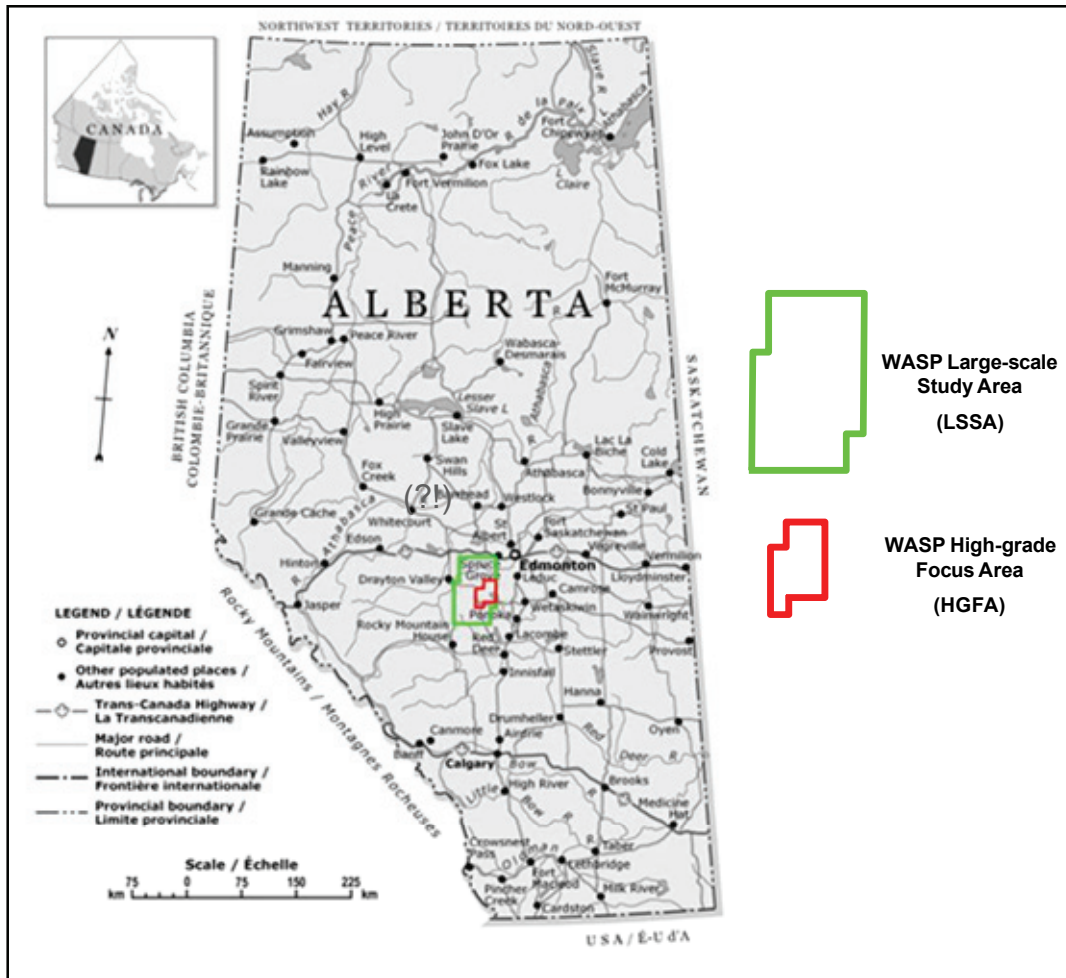


Figure 1: Location map of Wabamun Lake study area (NRCan, 2009).

WASP SEISMIC PROGRAM

Seismic characterization of the Nisku Formation in the Wabamun Area CO₂ Sequestration Project (WASP) high-grade focus area (HGFA) was based on analyzing and interpreting poststack seismic datasets comprising more than two hundred 2D seismic lines and seven 3D volumes. The study area is surrounded by two major hydrocarbon resources in Alberta; the Leduc reef play (east) and the Moon Lake reef play (northwest). Thus, part of the study area was mapped using vintage surface seismic data that had been acquired as part of hydrocarbon exploration in the area. The 2D and 3D seismic datasets have different acquisition and processing specifications and were acquired over many years prior to this project being undertaken. Therefore, prior to interpretation, inversion and attribute analysis, two primary steps were undertaken: data calibration and amplitude normalization. These steps were necessary to account for the vintage and datum differences within the data.

Table 1 gives an outline of the volume and approximate areal coverage of the analyzed seismic data as well as the number of wells with appropriate log curves and formation tops that were available for integration into the seismic data analysis. No new seismic data were acquired as part of Phase I of the project. The spatial distribution of the available seismic data is illustrated in Figure 3, and shows that the data coverage is not distributed uniformly. Thus characterization was constrained to those areas with good coverage. The 2D seismic data were used primarily for identifying long-wavelength structures, whereas the high-quality 3D data were used for detailed mapping, inversion and generation of seismic attributes.

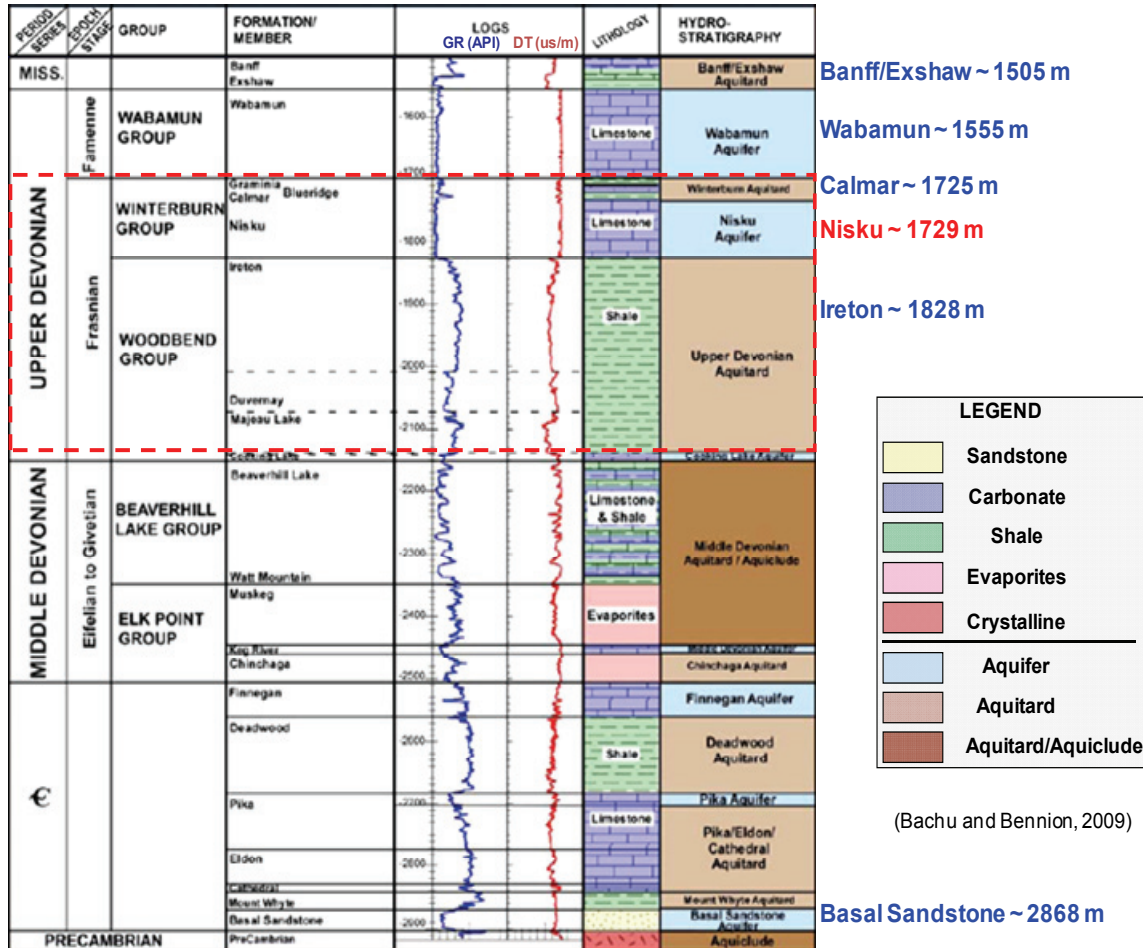


Figure 2: Stratigraphic model of Paleozoic strata in the study area using well 10-05-052-2W5 (Bachu and Bennion, 2009).

Table 1: Summary of the available seismic and wireline data. HGFA refers to the WASP high-grade focus area. * The borehole data referred to here are those with both sonic log and Ireton tops.

Seismic data	2D	200 seismic lines; approximately 2432 km in length
	3D	7 seismic volumes covering an area of 419 km ²
Borehole data*	Within HGFA	7 wells. Only 2 of which coincide with seismic coverage
	Nearby HGFA	Over 15 wells. Only 6 coincide with seismic coverage

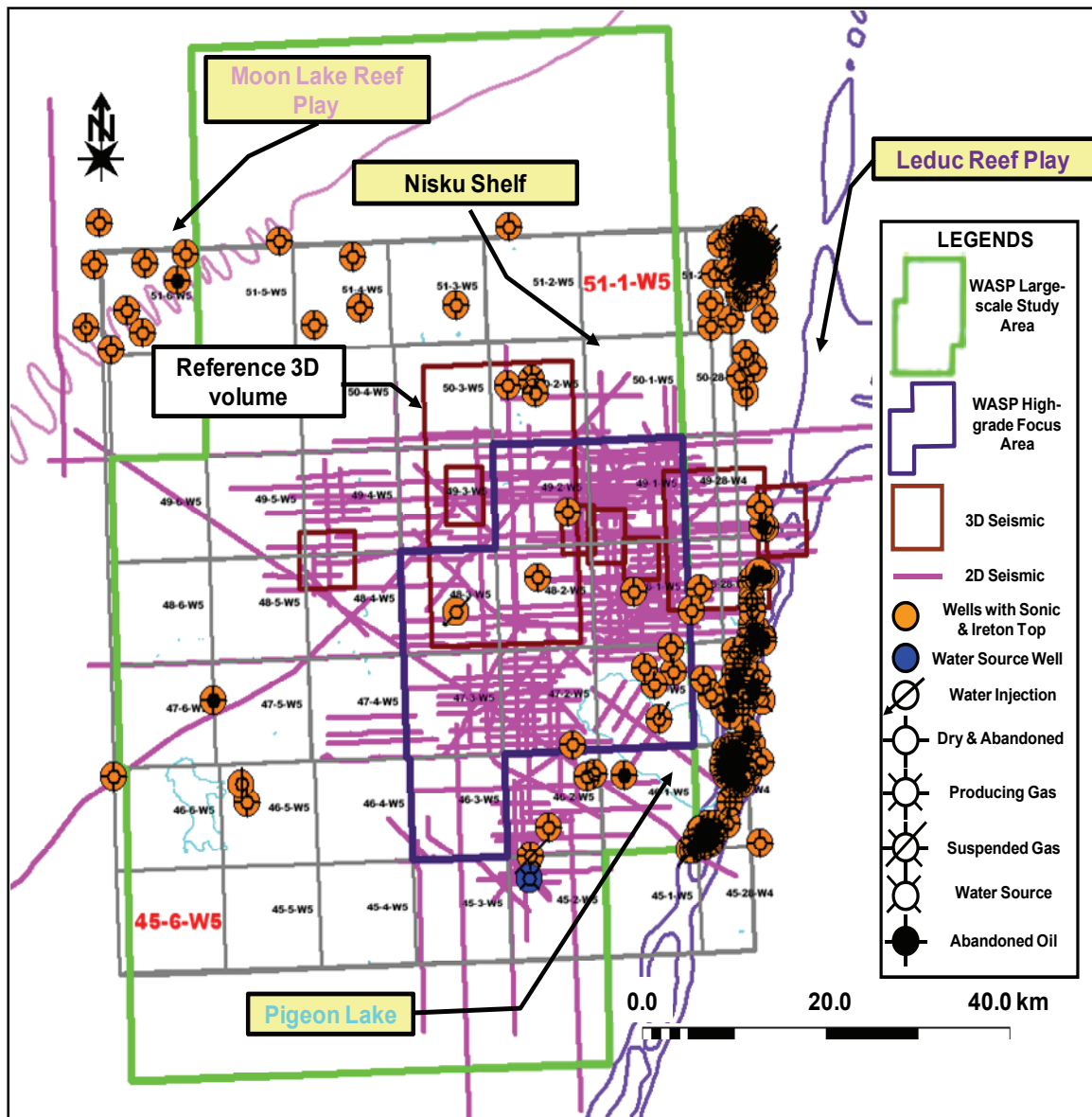


Figure 3: Base map showing the distribution of the seismic and borehole data. Cyan shapes indicate bodies of water.

METHOD: ACOUSTIC IMPEDANCE INVERSION

Acoustic impedance is one of the most useful seismic attributes as it yields distribution of pseudo-physical properties rather than a set of observations pertaining to the physical properties distribution. However, acoustic impedance requires good estimation of parameters as well as high quality seismic data and a good distribution of well control. Furthermore, inversion suffers from non-uniqueness.

In this project, various post-stack acoustic impedance inversion techniques were tested and only two were found to produce useful results: bandlimited and model-based inversions. Bandlimited inversion, also known as recursive inversion, is constrained mainly by the bandwidth of the seismic data, which typically falls between 7 and 60 Hz. The method estimates the acoustic impedance recursively by first extracting an estimate of the reflection coefficient from the seismic data and then re-arranging the normal incidence reflection coefficient relation to solve for the acoustic impedance of the $n^{\text{th}}+1$ layer (Z_{n+1}) (Cooke and Schneider, 1983):

$$R_n = \frac{Z_{n+1} - Z_n}{Z_{n+1} + Z_n} \xrightarrow{\text{solving for } Z_{n+1}} Z_{n+1} = \frac{Z_n(1+R_n)}{1-R_n}$$

Where R_n is the reflection coefficient of the n^{th} layer, Z_n is the acoustic impedance of the n^{th} layer ($\text{kg/m}^2\cdot\text{s}$), and n is a positive integer. Recall that the acoustic impedance of the n^{th} layer is its P-wave velocity (m/s) multiplied by its density (kg/m^3), i.e. $Z_n = \alpha_n \times \rho_n$.

Model-based inversion uses a different approach. First, the well control and the seismic data (horizons) are used to build an initial low-frequency estimated model of the acoustic impedance distribution. Using an estimate of the source wavelet, the model is then perturbed and the model response, in the form of synthetic seismogram, is measured. The model responses are then compared to the actual seismic traces, usually by means of crosscorrelation. The process is iterated until the model converges, i.e. the model response becomes within a predefined acceptable range from the actual observation. The misfit error between the two is quantified through various means; one of the most commonly used measures is the sum of the squared differences (Lines and Treitel, 1984).

There are many elements that could degrade the reliability of the inversion results, some of which could not be controlled, such as noise, whereas others could not be precisely calculated, such as the source wavelet. However, each method has its own advantages and disadvantages in regard to those limitations and it is suggested that by using both methods some of the ambiguities associated with the inversion results could be minimized. More information about those and other inversion methods can be found in Waters (1978), Aki and Richards (1980), Lines and Treitel (1984), Russell (1988), and the STRATA software theory manual. Figure 4 depicts some of the major steps adopted in the acoustic impedance inversion framework.

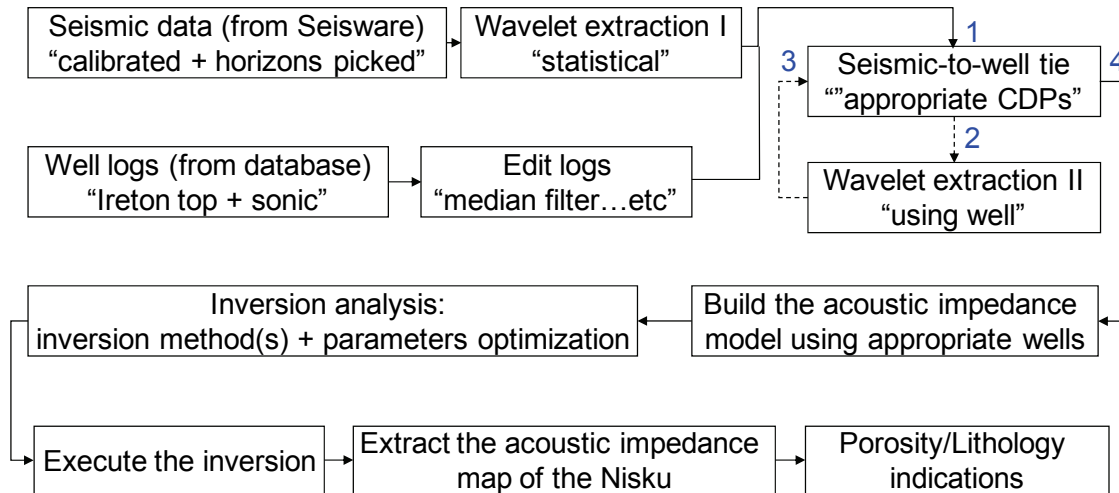


Figure 4: Flowchart outlining the major steps followed in the seismic inversion to extract the acoustic impedance map of the Nisku event.

RESULTS

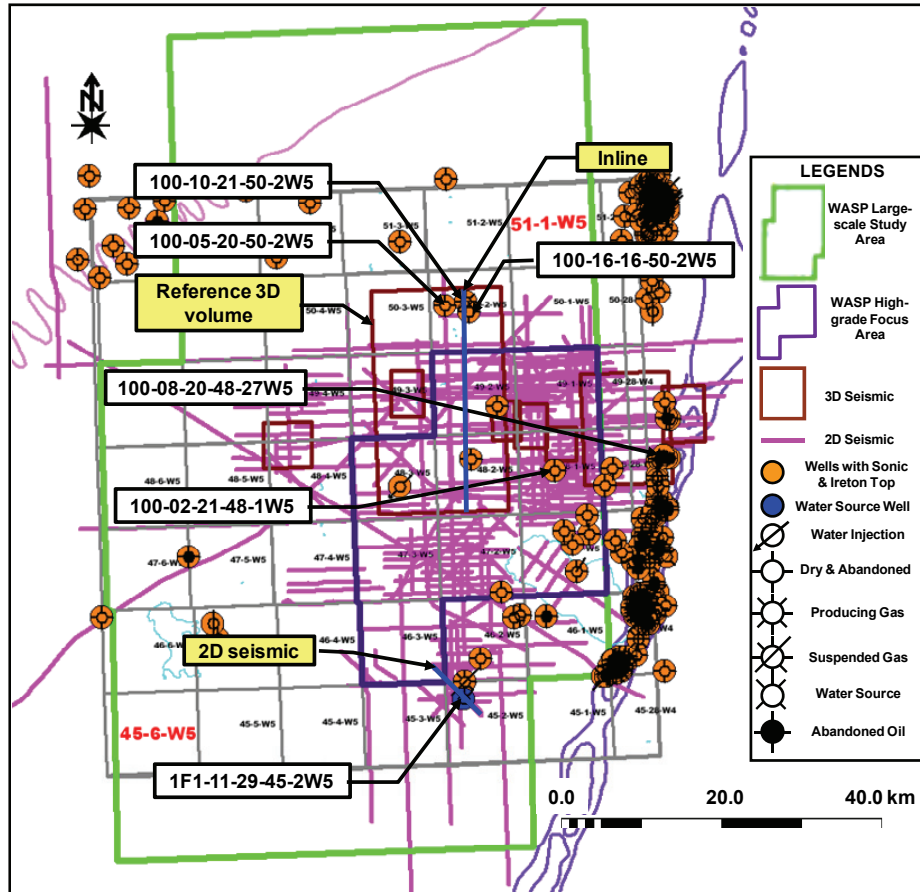
Field Data

A critical factor to achieving good inversion results is the seismic-to-well tie. The correlation coefficients associated with the wells used in the inversion are shown in Figure 5. Figure 6 shows example of the seismic-to-well tie near the water source well (1F1-11-29-45-2W5), at which a very good correlation is obtained (0.92). Prior to showing the Nisku acoustic impedance map, two examples were selected to illustrate the performance of each of the inversion methods. The first example is from the 2D seismic line near the water source well (Figure 7) while the other is from an inline extracted from the reference 3D volume (Figure 10). Figure 8 and Figure 11 show the initial “guess” model for the 2D and the extracted inline seismic sections while the inversion results using bandlimited and model-based inversion for those two sections are illustrated in Figure 9 and Figure 13, respectively.

The bandlimited inversion appears to produce a more detailed acoustic impedance model than the model-based inversion. For instance, the Wabamun and the Nisku formations are clearly separated by low impedance in the bandlimited inversion whereas they are hardly separated in the model-based inversion results (Figure 9 and Figure 13). However, for the acoustic impedance of the Nisku Formation, both methods yield similar results (Figure 13 and Figure 14), the only apparent difference being in the magnitude of the impedance. This is probably due to scaling differences. Furthermore, because there is a lack of well control, it is crucial that the impedance maps are interpreted only in terms of relative rather than absolute changes in acoustic impedance.

Several interesting low impedance zones are highlighted in Figure 13 and Figure 14. The impedance determination from the 2D seismic line near the water source well is also shown for comparison. By examining those maps, there seems to be two categories of low impedance: one that is associated with lithological/porosity changes in the Nisku Formation and another which is associated with discontinuities in the overlying

Wabamun event. Even though the results are not shown here, discriminating against the two groups of anomalies was achieved using coherency-sensitive methods. However, differentiation between acoustic impedance changes caused by enhanced porosity and those associated with a possible increase in shale content remains tenuous. With respect to the lithological/porosity changes, low acoustic impedance (Figure 13 and Figure 14) appears to normally correspond to low NRMS (Figure 15) while the time structure of the Nisku (Figure 16) is rather smooth and does not exhibit any significant variations within the WASP focus area expect for following the regional dip in the northeast-southwest direction.



Well	Seismic Reference	Correlation Coefficient
1F1-11-29-45-2W5	2D	0.92
100-10-21-50-2W5	3D	0.80
100-16-16-50-2W5	3D	0.83
100-05-20-50-2W5	3D	0.72
100-02-21-48-1W5	3D	0.63
100-08-20-48-27W4	3D	0.80

Figure 5: Correlation coefficient, over designed correlation window, between seismic data and synthetic seismogram from selected wells within the study area. The wells location are shown in the base map. The blue lines show the location of the 2D seismic (Figure 7) and the inline (Figure 10) invoked in the inversion.

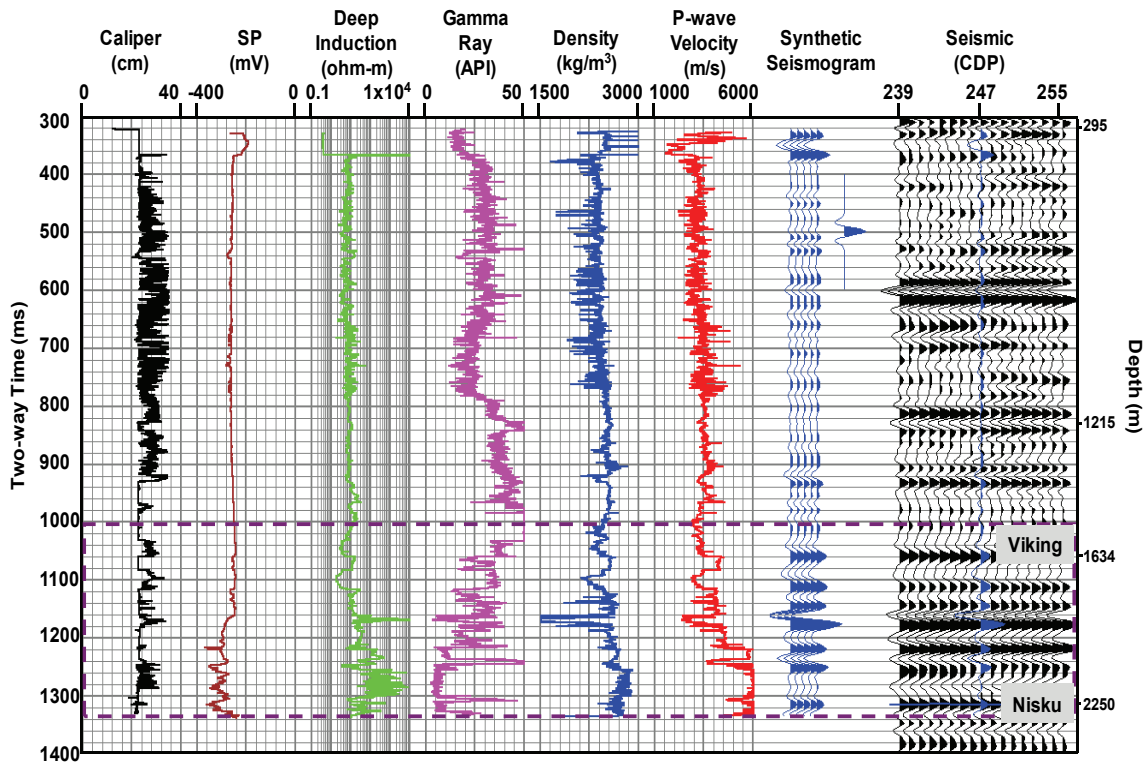
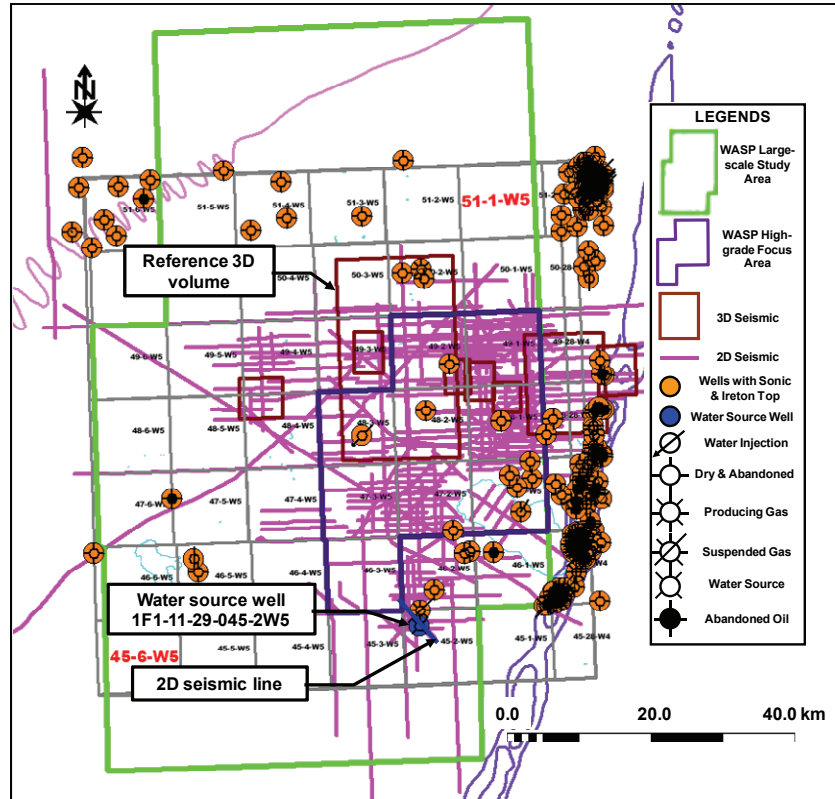


Figure 6: Seismic-to-well tie at the water source well (1F1-11-29-45-2W5). The location of the well and the seismic (blue) line are shown in the top image. The correlation coefficient is 0.92 over the outlined zone (dashed rectangle) in the bottom image.

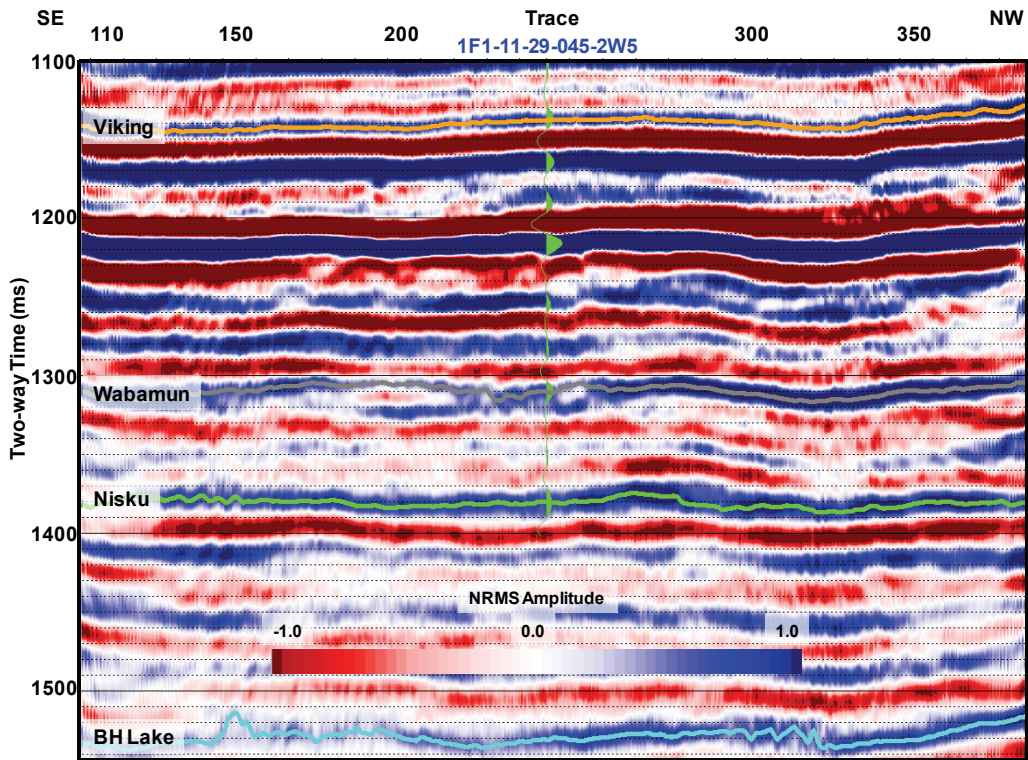


Figure 7: Seismic section near the water source well (Figure 5). The green curve at the well location is the correlated synthetic seismic trace. The correlation coefficient is 0.92.

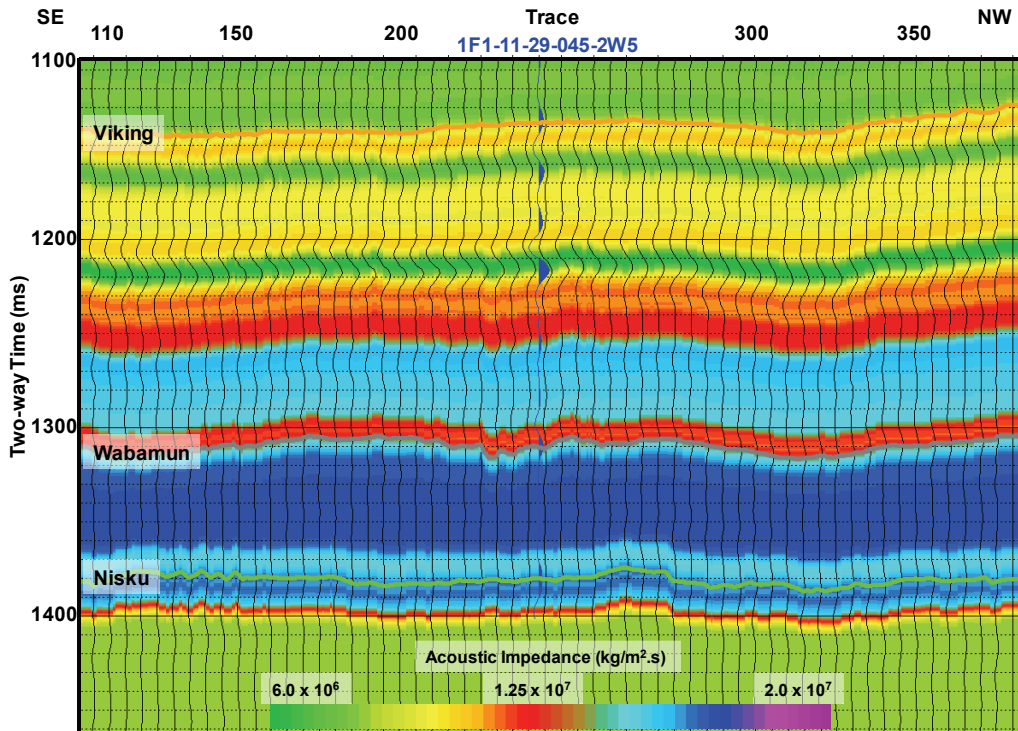


Figure 8: The initial acoustic impedance model of the seismic section in Figure 7. The blue curve at the well location is the correlated synthetic seismic trace while the black curves are the actual seismic traces.

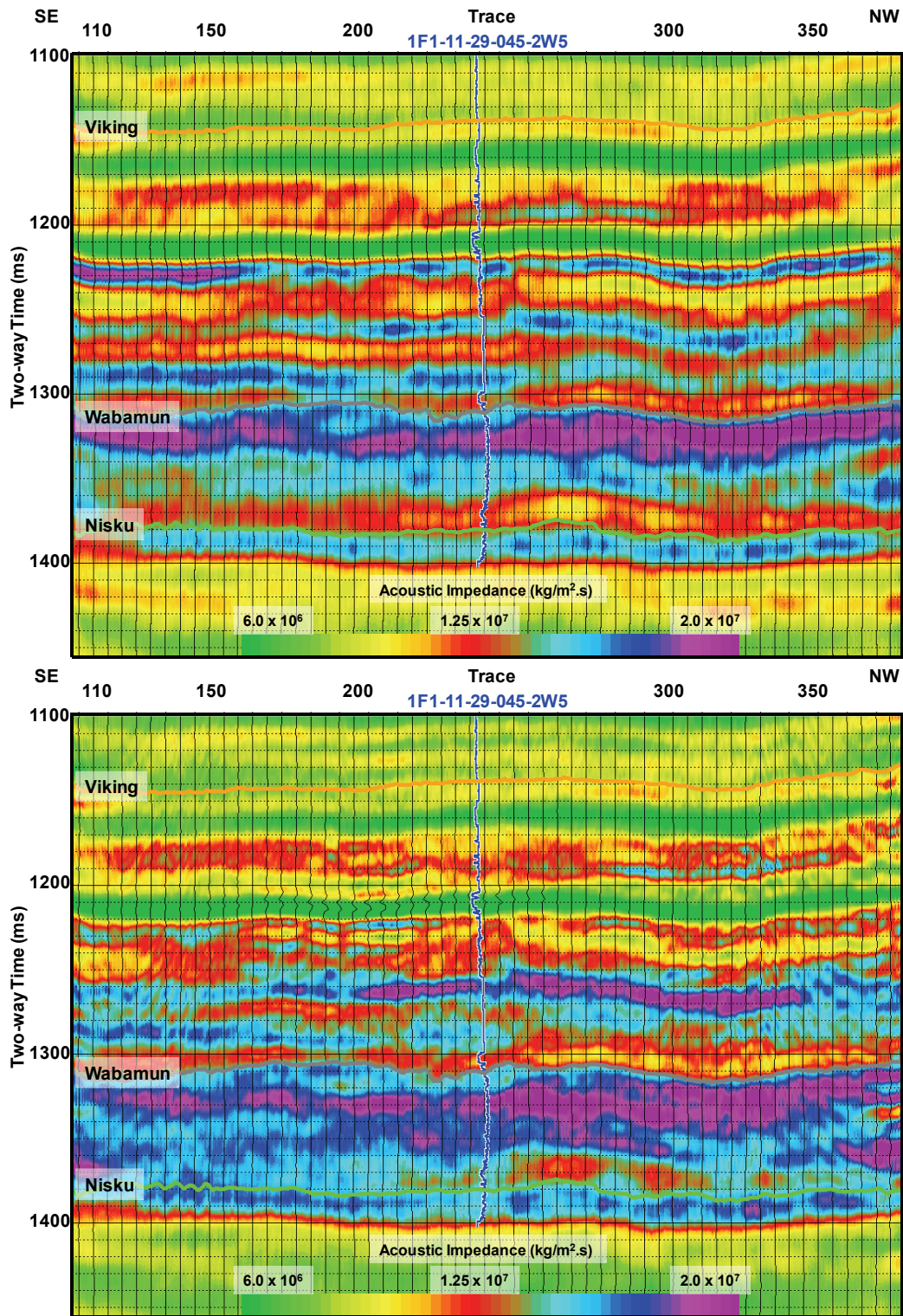


Figure 9: Estimated acoustic impedance along the 2D seismic line near the water source well (Figure 5) using bandlimited (top) and model-based (bottom) inversion methods. The inserted blue curve at the well location represents the computed acoustic impedance from the sonic and density logs. The black curves represent the acoustic impedance from the bandlimited inversion whereas in the model-based inversion they represent the misfit error.

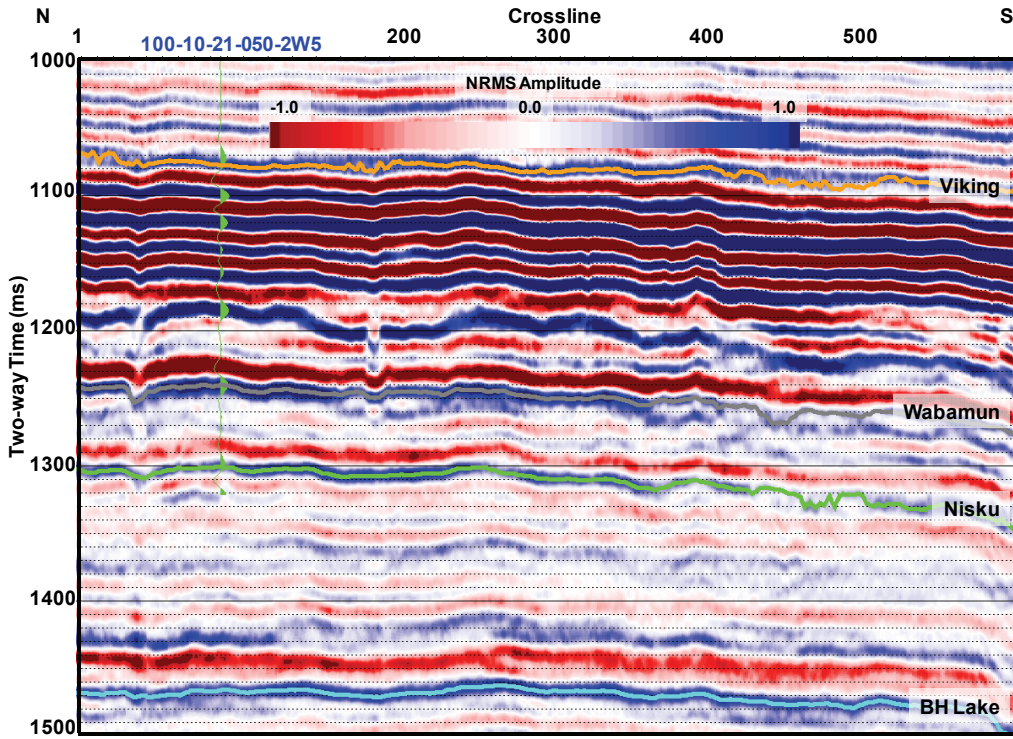


Figure 10: Inline extracted from the reference 3D seismic volume (Figure 5). The green curve at the well location is the correlated synthetic seismic trace. The correlation coefficient is 0.80.

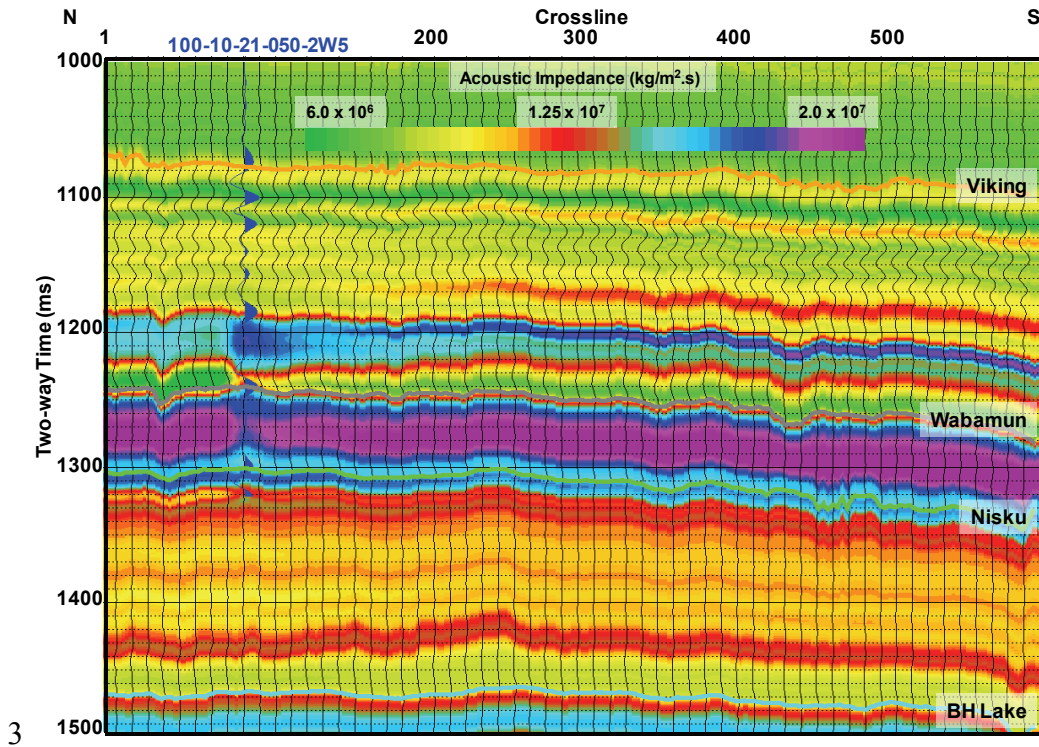


Figure 11: The initial acoustic impedance model corresponding to the inline in Figure 10. The blue curve at the well location is the correlated synthetic seismic trace while the black curves are the actual seismic traces.

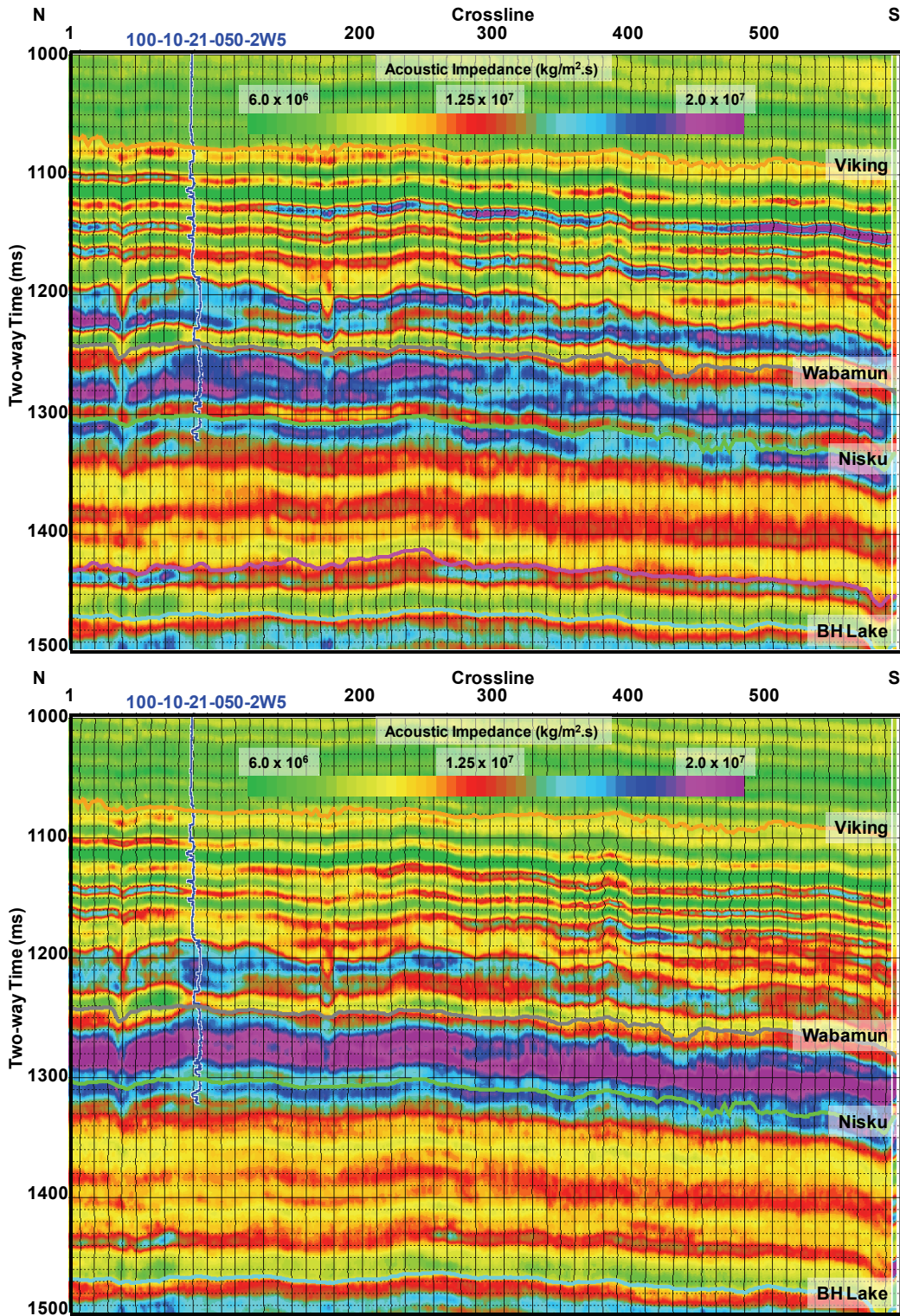


Figure 12: Estimated acoustic impedance of the inline in Figure 10 and Figure 11 using bandlimited (top) and model-based (bottom) inversion methods. The inserted blue curve at the well location represents the computed acoustic impedance from the sonic and density logs. The black curves refer to the acoustic impedance from the bandlimited inversion whereas in the model-based inversion they represent the misfit error.

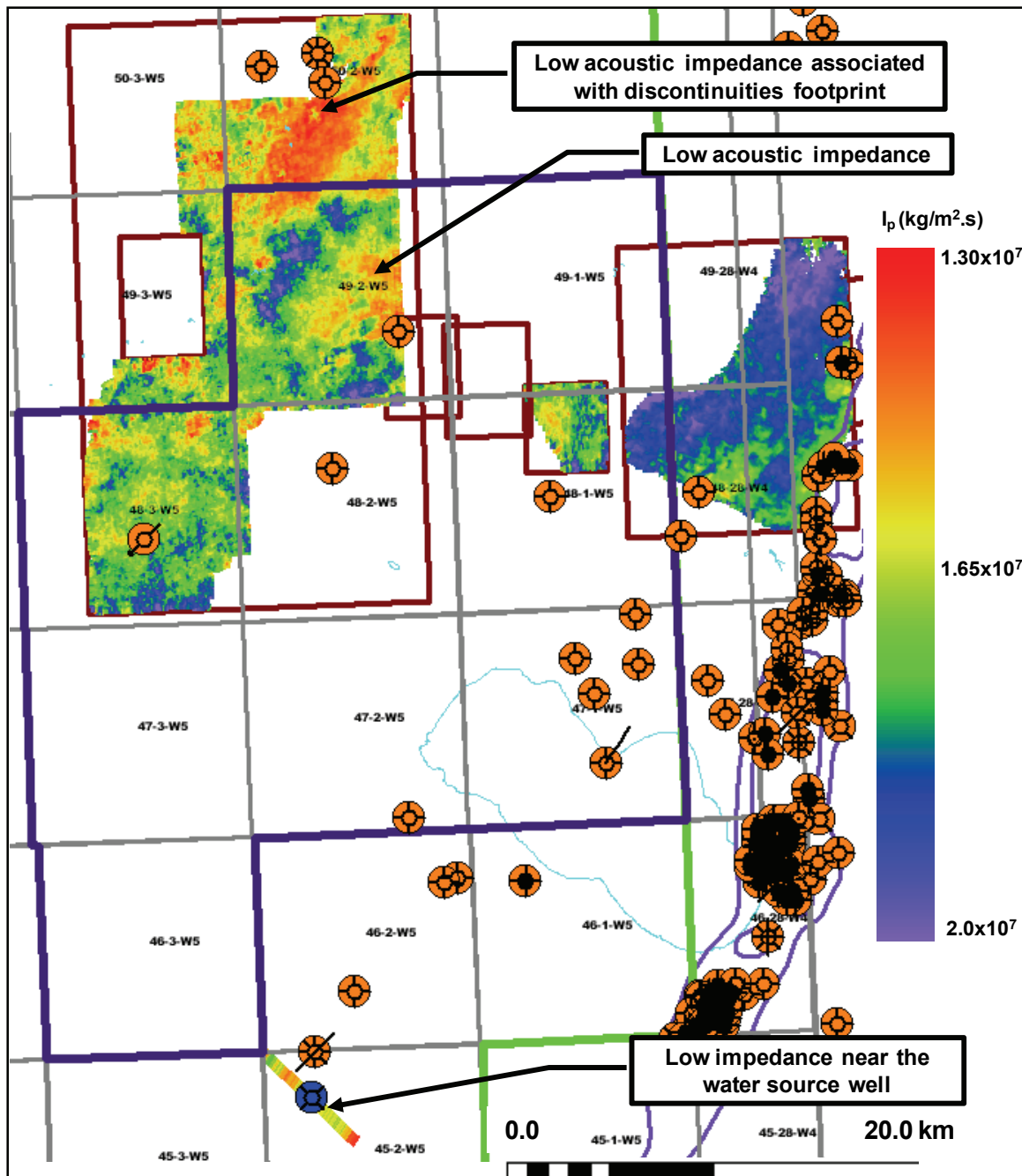


Figure 13: Estimated Acoustic impedance (I_p) map of the Nisku Formation using bandlimited inversion. Due to lack of well control, the inversion was not performed on the entire dataset.

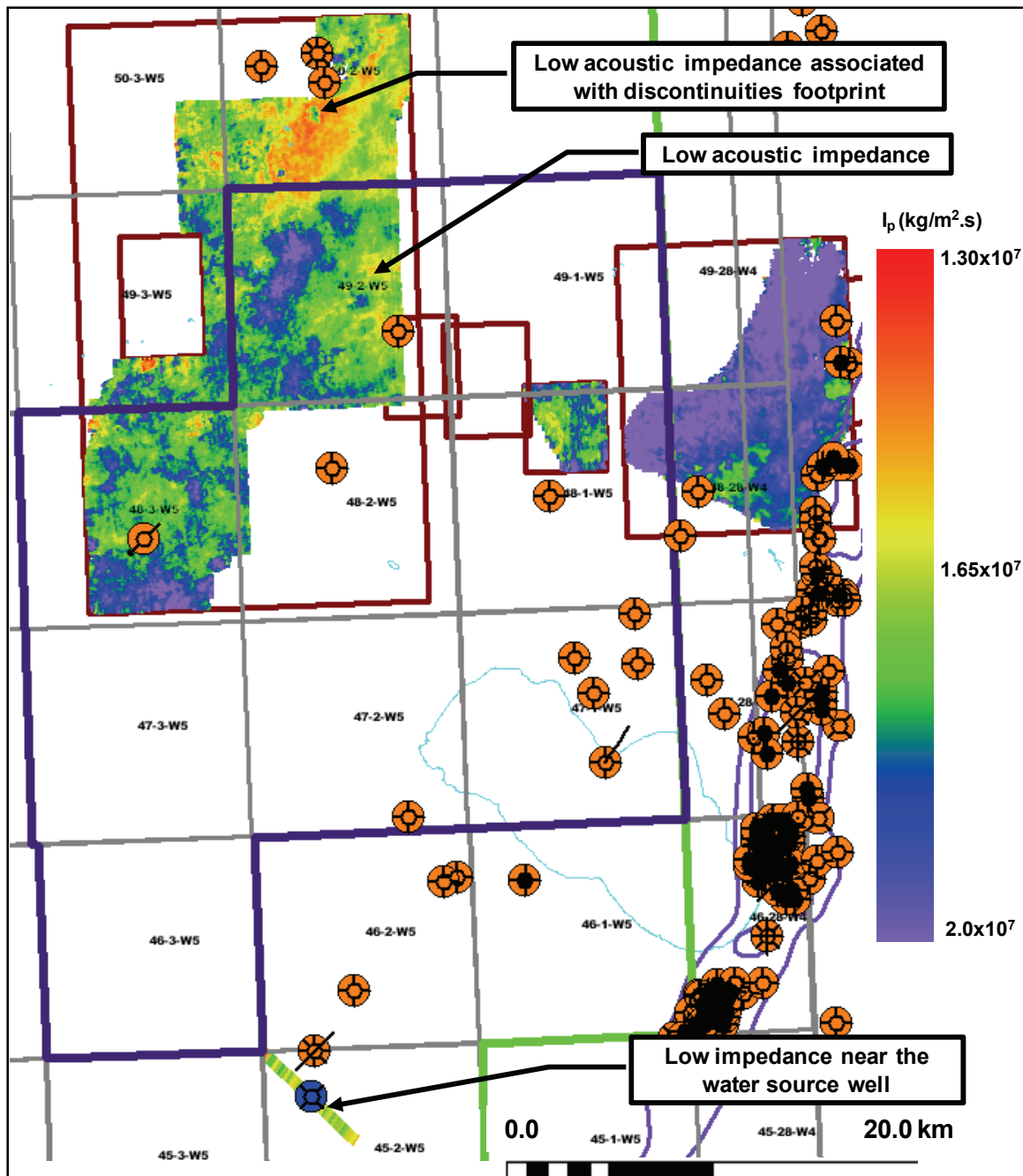


Figure 14: Estimated Acoustic impedance (I_p) map of the Nisku Formation using model-based inversion. Due to lack of well control, the inversion was not performed on the entire dataset.

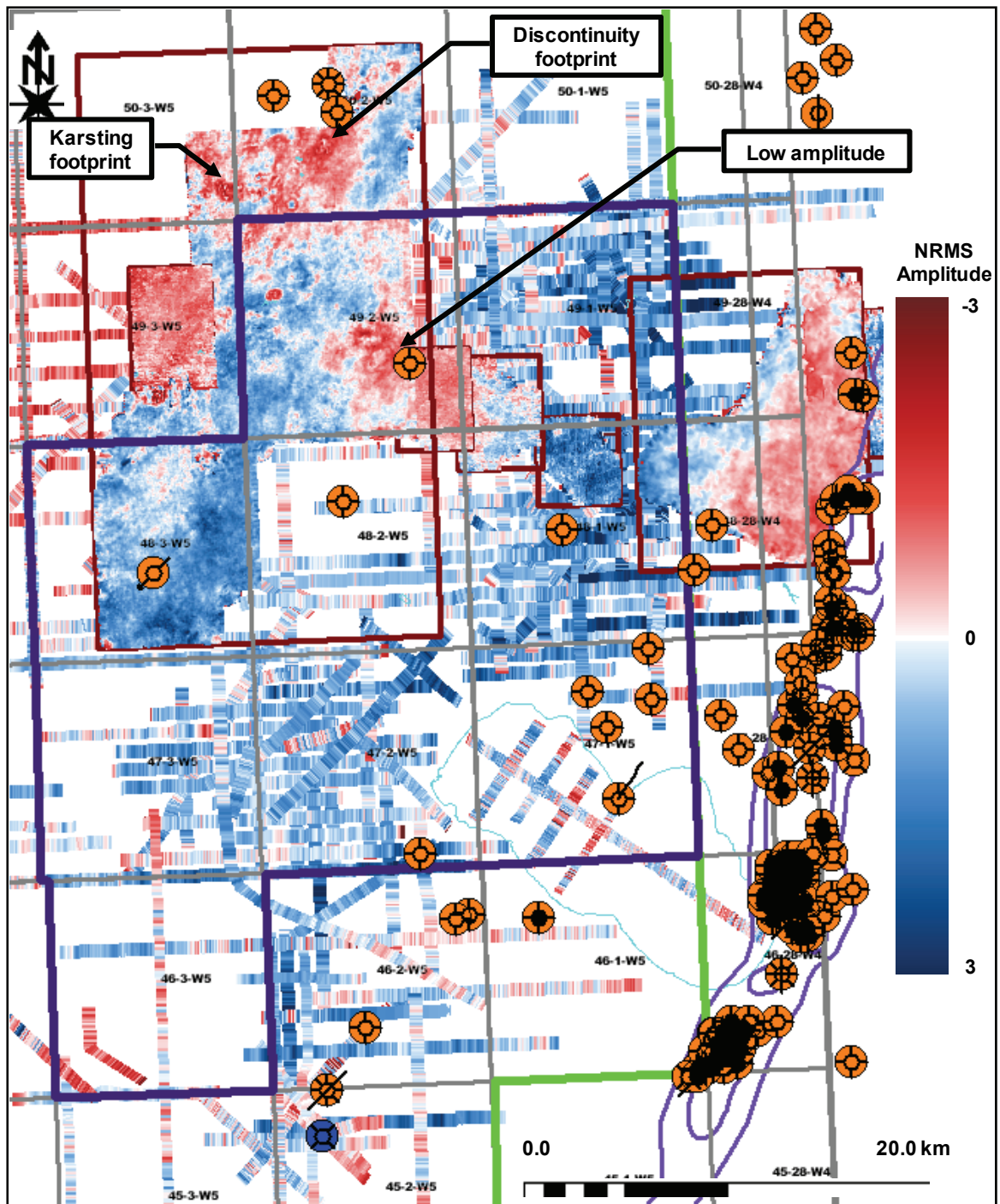


Figure 15: Nisku NRMS amplitude map. Some of the major amplitude anomalies are specified: Wabamun karsting footprint, Wabamun discontinuities footprints, and the Nisku amplitude low. It should be emphasized that the karsting and discontinuities shown here are just due to the footprint of those anomalies and do not indicate that the Nisku has been physically affected.

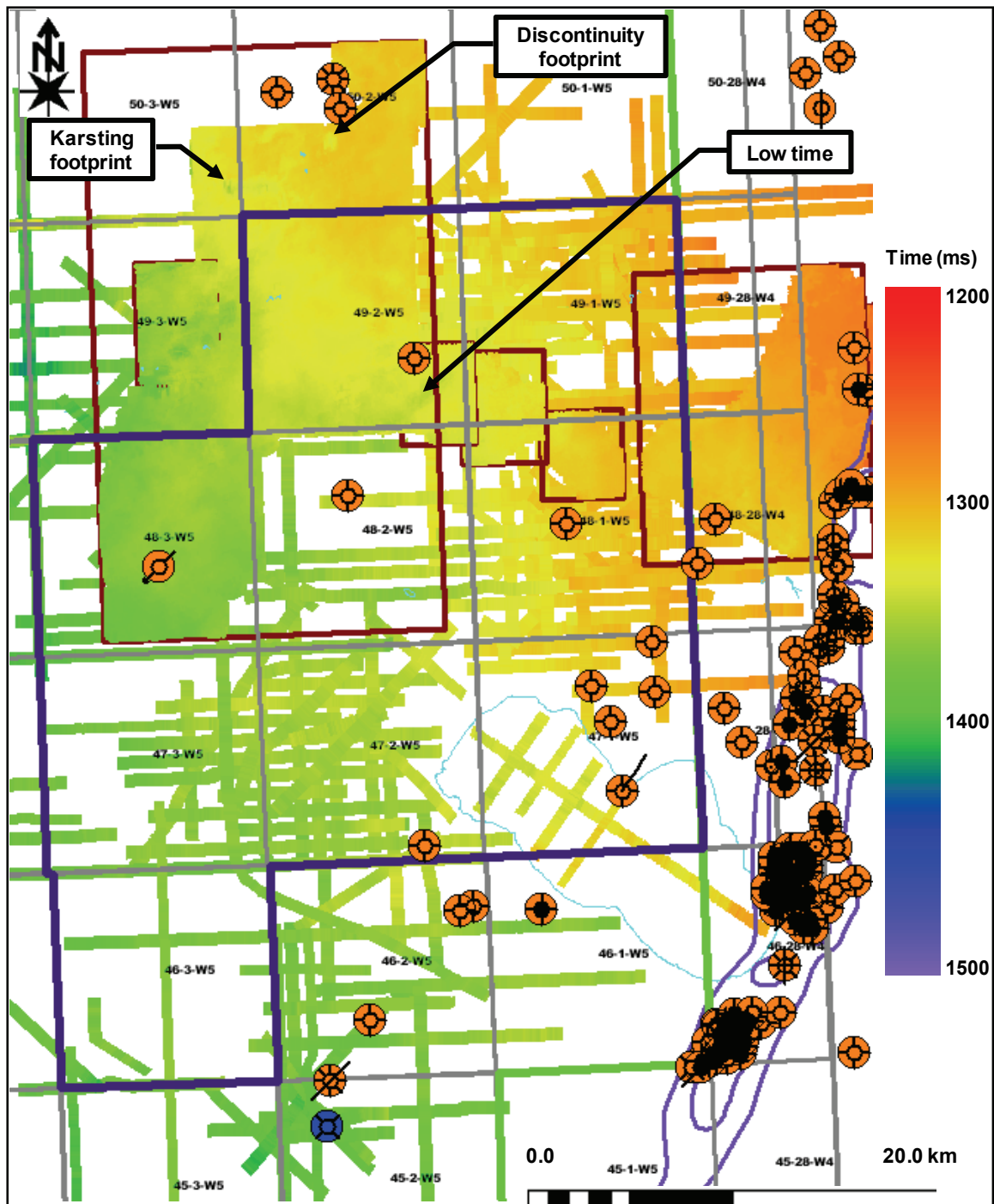


Figure 16: The Nisku time structure map. The locations of some of the major anomalies are specified: Wabamun karsting footprint, Wabamun discontinuities footprints, and the Nisku local time low. It should be emphasized that the karsting and discontinuities shown here are due to the footprint of those anomalies and do not indicate that the Nisku has been physically affected.

Synthetic Data

There are several factors that could affect the acoustic impedance of the Nisku event as observed in the field data. Therefore, some sensitivity analyses were undertaken and it was found that thickness and average P-wave velocity are the primary parameters affecting the Nisku event impedance. Subsequently, zero-offset synthetic seismograms were generated using a 25 Hz Ricker wavelet and the convolutional model to further understand the effect of these two parameters on the Nisku event acoustic impedance. Figure 17 is a side-by-side panel display illustrating the thickness and average P-wave velocity effect on the Nisku event amplitude whereas Figure 18 shows a display of the Nisku event amplitude as a function of those two parameters. Changing the average P-wave velocity (vertical axis) will cause over a 60% change in the amplitude whereas changing the thickness (horizontal axis) will only cause about an 8% variation in amplitude (Figure 15).

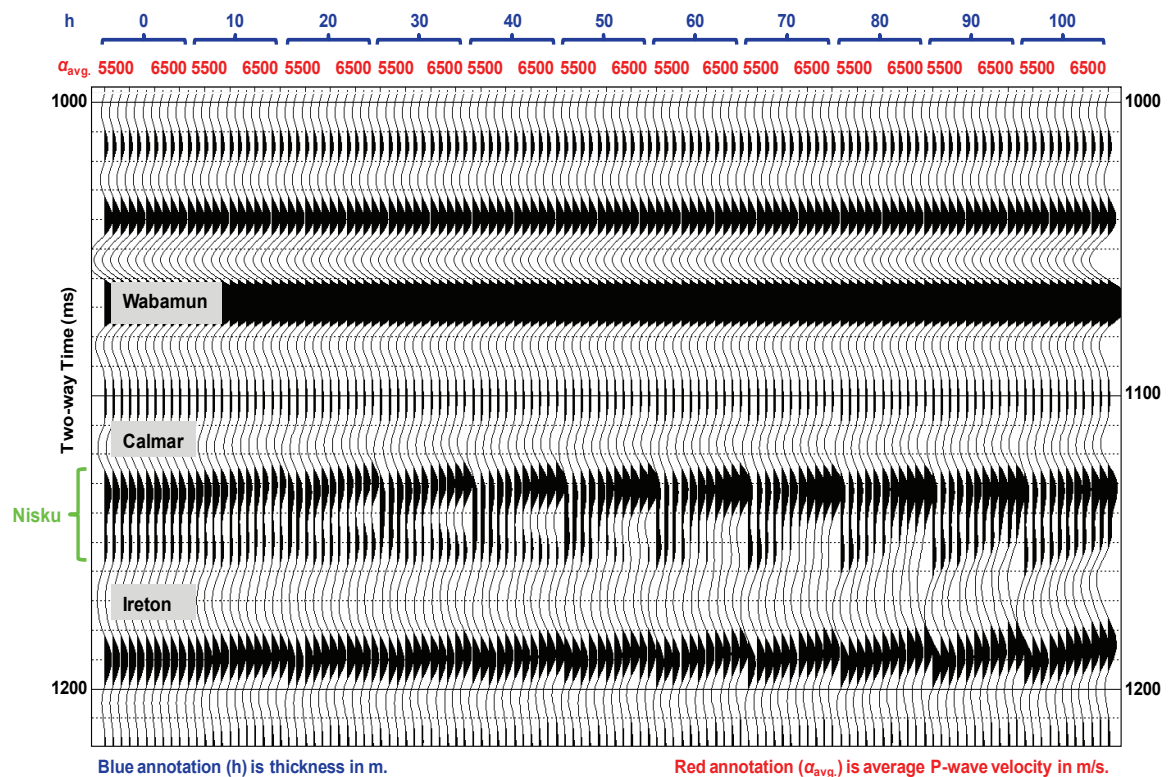


Figure 17: Sequential display of normal incidence synthetic seismograms in which the Nisku event amplitude is modelled as function of thickness and average P-wave velocity. The top of the Nisku event is identified as the peak at approximately 1130 ms (the green bracket along the time axis approximates the frequency cycle through the formation). In each blue bracket (thickness effect), there are 11 traces, each representing the seismic amplitude associated with that thickness and an average Nisku P-wave velocity increasing from 5500 m/s to 6500 m/s at an increment of 100 m/s. The modelling was undertaken using well 100-10-05-052-02W5. The actual Nisku thickness and average P-wave velocity at this well are 100 m and 6100 m/s, respectively.

To relate variations in the acoustic impedance to the two primary physical parameters of interest, i.e. thickness and average P-wave velocity, the acoustic impedance of the synthetic seismogram in Figure 17 was reconstructed using bandlimited and model-based inversion methods (Figure 19). The modelling results suggest that the acoustic impedance variations in the study area, excluding those associated with karsting and discontinuities footprints, are most likely due to variability in the average P-wave velocity (i.e. lithology and/or porosity) rather than thickness.

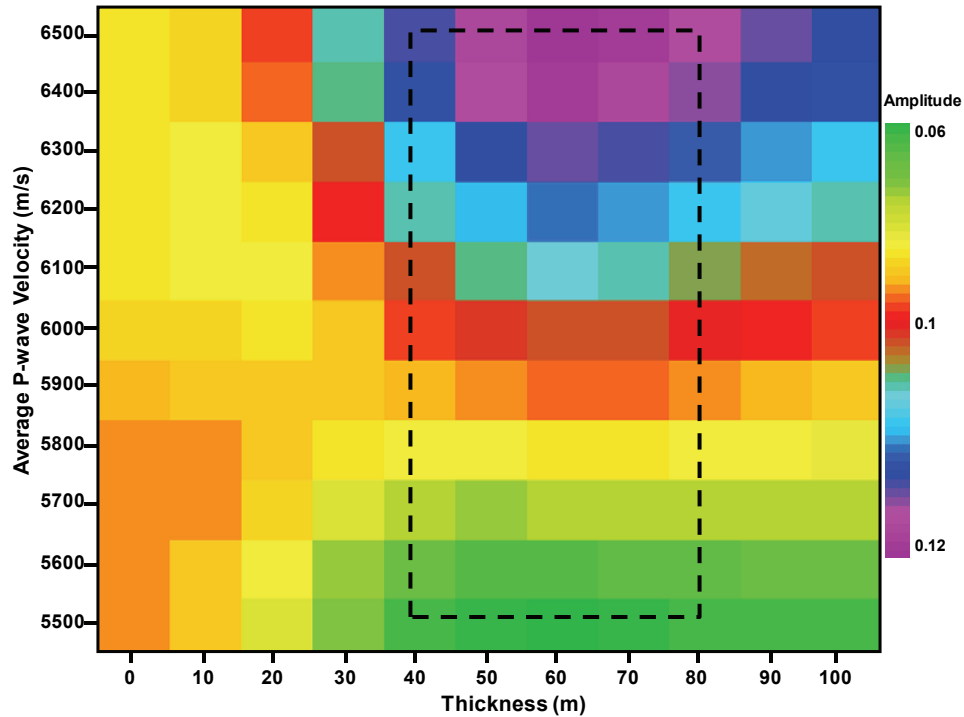


Figure 18: Nisku event amplitude as a function of thickness and average P-wave velocity synthetic modelling. The actual Nisku thickness and average P-wave velocity are 100 m and 6100 m/s, respectively. The maps represent the Nisku amplitude map that resulted from picking the peak amplitude corresponding to the Nisku event in Figure 17. The black dashed rectangle outlines the most likely Nisku thickness and average velocity values within the study area based on well control. The results suggest that the Nisku average P-wave velocity (or impedance) effect is more significant than the thickness effect. Thus, the highest sensitivity is along the vertical axis.

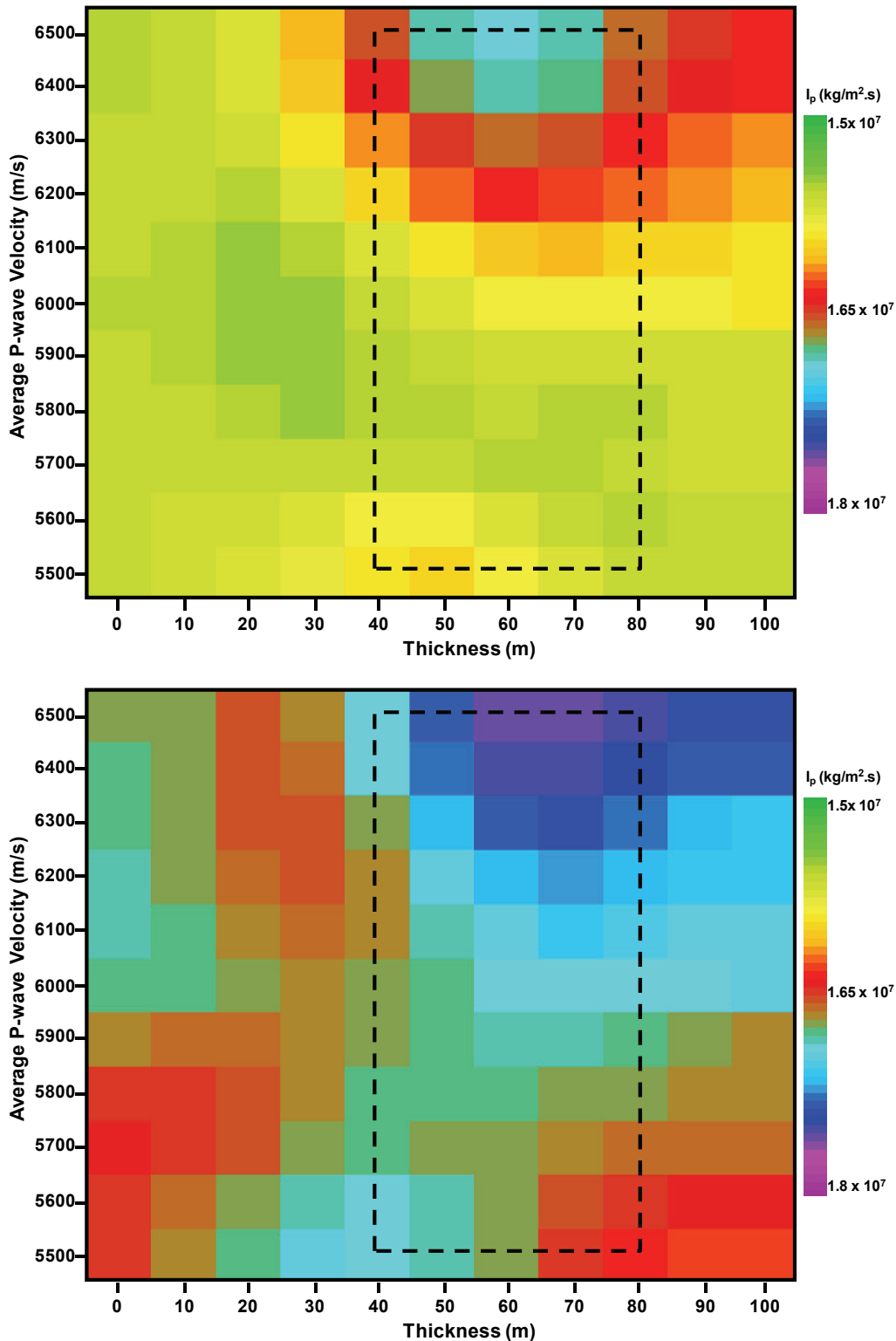


Figure 19: Acoustic impedance (I_p) of the synthetic seismogram in Figure 17 using bandlimited (top) and model-based (bottom) inversion methods. Similar to the seismic amplitude response, the acoustic impedance shows high sensitivity toward variations in the Nisku Formation average P-wave velocity rather than thickness. The maps illustrate the direct proportionality between average P-wave velocity and acoustic impedance. Note the similarity in the results except for the small difference in the magnitude of the acoustic impedance due to scaling issues.

CONCLUSIONS

The acoustic impedance map of the Nisku event shows strong variations across the WASP study area. Our interpretation indicates that there are two categories of low impedance: one that is associated with lithological/porosity changes in the Nisku Formation and another which is associated with discontinuities in the overlying Wabamun event. In addition to the time structure, NRMS amplitude and coherency-sensitive attributes, forward and inverse seismic modelling were undertaken in delineating anomalies caused by lithological variations in contrast to those induced by geological discontinuities. The modelling results suggest that variation in the average P-wave velocity is the primary physical parameters steering the acoustic impedance of the Nisku event. Consequently, several favourable zones of low acoustic impedance are identified in the study area. However, differentiation between acoustic impedance changes caused by enhanced porosity and those associated with a possible increase in shale content remains tenuous.

ACKNOWLEDGEMENT

We thank WASP sponsors and the Natural Sciences and Engineering Research Council of Canada (NSERC) for funding the project and the WASP technical team for valuable discussions, ENCANA kindly provided access to the seismic data, and Jimmy Haszard (ENCANA), Jay LeBlanc (ENCANA), and Ian Reglar (formerly ENCANA) provided valuable technical support. Hampson-Russell, Seismic-Micro Technology and Zokero are thanked for providing seismic interpretation software. We also acknowledge the continuing support of CREWES sponsors.

REFERENCES

- Aki, K., Richards, P.G., 1980. Quantitative Seismology, Freeman and Co., New York.
- Bachu, Stefan and Bennion, Brant, 2009, Effects of In-situ Conditions on Relative Permeability Characteristics of CO₂-Brine System: <<http://www.gwpc.org/e-library/documents/co2/LBNL%20CO2%20Effects%20of%20Insitu%20Conditions%20on%20Permeability.pdf>>.
- Cooke, D. A., and Schneider, W. A., 1983, Generalized linear inversion of reflection seismic data: *Geophysics*, 48, 665-676.
- Lines, L. R., and Treitel, S., 1984, A review of least-squares inversion and its application to geophysical problems: *Geophysical Prospecting*, 32, 159-186.
- Russell, B.H., 1988, Introduction to seismic inversion methods: Society of Exploration Geophysicists, Course Notes Series, No. 2, S. N. Domenico, Series Editor.
- Sherriff, R. E., 1991. *Encyclopedic Dictionary of Exploration Geophysics*: Society of Exploration Geophysicists, 4th edition, Tulsa, Oklahoma.
- Michael, K., S. Bachu, B. Buschkuhle, K. Haug, and S. Talman, 2008, Comprehensive Characterization of a Potential Site for CO₂ Geological Storage in Central Alberta, Canada: AAPG Manuscript, 40 p.
- Natural Resources of Canada, 2009, <http://atlas.nrcan.gc.ca/site/english/maps/reference/provinceterritories/alberta/referencemap_image_view>.
- Waters, K. H., 1978, *Reflection seismology*: John Wiley and Sons.
- Watts, N., 1987, Carbonate sedimentology and depositional history of the Nisku Formation in south-central Alberta, in F.F. Krause and O. G. Burrowes, eds., *Devonian lithofacies and reservoir styles in Alberta*: 2nd International Symposium of the Devonian System, 13th CSPG Core Conference, 87-152.